Effect of Ar–N_2 Sputtering Gas on Structure and Tunneling Magnetodielectric Effect in Co–(Si–N) Nanogranular Films

T. Uchiyama[1], Y. Cao[2], H. Kijima-Aoki[3], K. Ikeda[4], N. Kobayashi[4], S. Ohnuma[1,4], and H. Masumoto[1]

[1]Frontier Research Institute for Interdisciplinary Science, Tohoku University, Sendai 980-8578, Japan
[2]School of Materials Science and Engineering, Hubei University, Wuhan 430062, China
[3]Department of Electrical Engineering, Tohoku University, Sendai 980-8578, Japan
[4]Research Institute for Electromagnetic Materials, DENJIKEN, Tomiya 981-3341, Japan

We have investigated the effect of N_2 fraction x in Ar–N_2 sputtering gas on the tunneling magnetodielectric (TMD) effect in Co–(Si–N) nanogranular films. Co–(Si–N) films were deposited by co-sputtering Co and Si_3N_4 targets in Ar-x vol.%N_2 mixture gas with different N_2 gas fractions x of 0–30. All deposited films had a nanogranular structure composed of Co nanogranules with a diameter of 1–3 nm embedded in a Si–N matrix. We realized the TMD effect in the films for $x \geq 3.3$, and the film deposited in Ar-6.6 vol.%N_2 gas showed the highest dielectric variations in a magnetic field. For $3.3 \leq x \leq 10$, TMD peak frequency f_{TMD} decreased from 17 to 40 kHz with increasing x because of the increase in intergranular spacing s. On the other hand, for $10 < x \leq 30$, f_{TMD} increased from 40 kHz to 3.3 MHz as x increased since both s in the out-of-plane direction and β, which indirectly represents the measure of the distribution of s, decreased. This study provides a new way to tailor the frequency response of the TMD effect.

Index Terms— **Cobalt–silicon nitride, nanogranular film, sputtering method, tunnel magnetodielectric effect.**

I. Introduction

MAGNETOELECTRIC (ME) materials, which possess both magnetic and electric properties, have attracted much attention for their applications, such as magnetic memory and magnetic sensors. Magnetic metal–insulator nanogranular films, which consist of nanometer-sized magnetic metal (e.g., Co, Fe) granules embedded in an insulating (e.g., MgF_2, Al_2O_3) matrix, belong to ME materials and exhibit a variety of intriguing functionalities: high-frequency soft magnetic properties [1], [2], [3], Hall effect [4], [5], [6], tunnel magnetoresistance effect [7], [8], [9], tunnel magneto-optic effect [10], and giant Faraday effect [11]. Additionally, our group discovered a new ME effect, tunneling magnetodielectric (TMD) effect, which causes a magnetic field-induced increase in the dielectric permittivity of nanogranular films [12]. The TMD effect exhibits the frequency dependence. Upon the application of the magnetic field, there exists a maximum change in the dielectric permittivity at certain frequency of ac electric field. So, to control its frequency response is central to the regulation of the TMD effect toward real-world high-frequency device applications.

The TMD effect in nanogranular films originates from the tunneling oscillation of electrons between two magnetic metal granules through the insulating matrix. Therefore, the structure factors, such as phase separation and intergranular spacing (i.e., the spacing between granular surfaces) [13], [14], [15], as well as the intrinsic factors such as the heat of formation at 25 °C, ΔH, and the electrical resistivity, ρ, of the matrix [16], [17], are key to regulate the sensitivity and the frequency dependence of the TMD effect. So far, the TMD effect has been reported in fluoride-based nanogranular films (e.g., Co–(Al–F) [13], Co–(Mg–F) [14], [15], Co–(Sr–F) [16], and Co–(Ba–F) [18]) and oxide-based nanogranular films (e.g., Co–(Al–O) [17] and Co–(Si–O) [19]), whose matrices have high ΔH and ρ. However, there has been no report on the TMD effect in nitride-based nanogranular films. Nitride-based nanogranular films have an advantage over fluoride- and oxide-based films: instability of Co–N. Co–N has much lower ΔH ($\Delta H = -8$ kJ/mol [20]) than CoF_3 ($\Delta H = -782$ kJ/mol [20]) and Co_3O_4 ($\Delta H = -905$ kJ/mol [20]), so the degradation of magnetic properties is less likely to occur. We chose Co–(Si–N) system because of the high ΔH and ρ of Si_3N_4 ($\Delta H = -738$ kJ/mol [20], $\rho = 10^{17}$–10^{19} $\mu\Omega \cdot$ m [21], [22]). The large difference in ΔH between Co–N and Si_3N_4 would enable the formation of separated Co granules and the Si–N matrix. In addition, a Si_3N_4 matrix would function as the tunneling barrier owing to its high ρ. Another reason for choosing Co–(Si–N) films is that their intergranular spacing, which has a strong influence on the frequency response of TMD effect [14], [15], can potentially be controlled using the reactive sputtering method, as the structure of sputter-deposited films is highly sensitive to the composition of the sputtering gas. This can be achieved by employing a mixture of Ar–N_2 gas with varying N_2 gas fraction during the deposition process.

In this study, to realize the first TMD effect in nitride-based nanogranular films and to control the frequency dependence of TMD effect, we have deposited Co–(Si–N) nanogranular films and investigated the effect of N_2 fraction in Ar–N_2 sputtering gas on the structure and TMD effect of the films.

II. Experimental Procedure

Co_{19}–$(Si–N)_{81}$ nanogranular films were deposited on a Pt/Ti/Si (100) and quartz glass substrate by co-sputtering Co

Manuscript received 29 March 2023; revised 20 May 2023; accepted 29 May 2023. Date of publication 7 June 2023; date of current version 24 October 2023. Corresponding author: H. Masumoto (e-mail: hiromasu@fris.tohoku.ac.jp).

Color versions of one or more figures in this article are available at https://doi.org/10.1109/TMAG.2023.3283530.

Digital Object Identifier 10.1109/TMAG.2023.3283530

© 2023 The Authors. This work is licensed under a Creative Commons Attribution 4.0 License.
For more information, see https://creativecommons.org/licenses/by/4.0/

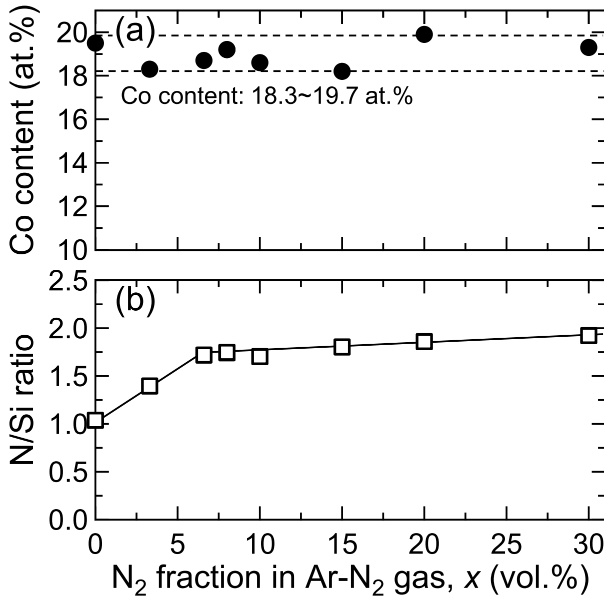

Fig. 1. N_2 gas fraction x dependence of (a) Co content and (b) N/Si ratio of Co–(Si–N) films.

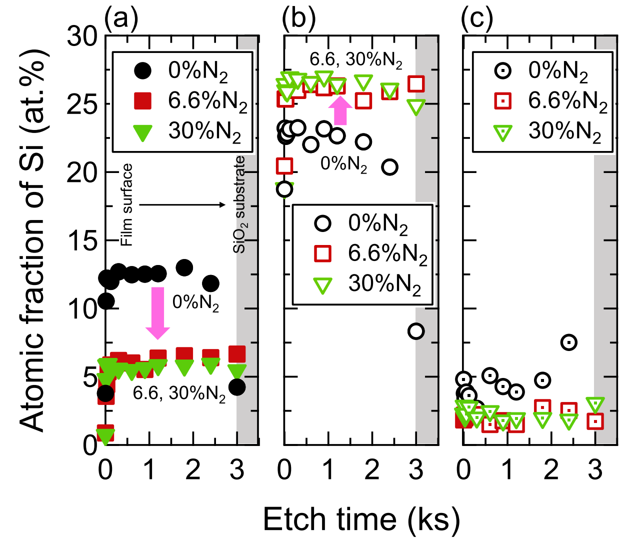

Fig. 2. XPS depth profile of (a) metal Si, (b) Si–N, and (c) Si–O in Co_{19}–$(Si–N)_{81}$ films deposited in Ar-0, 6.6, and 30 vol.%N_2 gas.

and Si_3N_4 targets at 0.2 Pa of Ar-x vol.%N_2 ($0 \leq x \leq 30$, N_2 gas fraction in Ar–N_2 sputtering gas) mixture gas atmosphere. The substrate temperature was kept at 400 °C during deposition. The film thickness was 650 ± 50 nm.

The film composition and the chemical states of the elements in the films were detected with X-ray fluorescence and X-ray photoelectron spectroscopy (XPS), respectively. The crystal structure and morphology of the films were observed with transmission electron microscopy (TEM). The electrical resistivity in the in-plane direction was measured using the four-probe method. The magnetization curve in the in-plane direction was measured with a vibrating sample magnetometer. Permittivity ε in the out-of-plane direction was evaluated with an impedance analyzer from 0.01 to 100 MHz with and without an external magnetic field H up to 800 kA/m. Herein, H was applied to the films in the in-plane direction. TMD response was calculated using

$$\text{TMD ratio} = \frac{\varepsilon'_H - \varepsilon'_0}{\varepsilon'_0} \tag{1}$$

where ε'_H and ε'_0 are the real parts of ε with and without H. All measurements were conducted at room temperature.

III. Results and Discussion

A. Composition and Structure

Fig. 1 shows the N_2 gas fraction, x, dependence of (a) Co content and (b) N/Si ratio of Co–(Si–N) films. Co contents of all films were confirmed to retain a very small composition deviation of 19 ± 0.7 at.%. N/Si ratio increased dramatically with increasing x from 0 (N/Si = 1.03) to 6.6 vol.% (N/Si = 1.72) and then increased slightly with increasing x from 6.6 to 30 vol.% (N/Si = 1.92). Fig. 2 shows the XPS depth profile of Si in Co_{19}–$(Si–N)_{81}$ films deposited in Ar-0, 6.6, and 30 vol.%N_2 gas. According to the XPS analysis, Si in the films existed in three states: metal Si, Si–N, and Si–O. The atomic fraction of metal Si decreased with increasing x from 0 to 6.6 vol.%. On the other hand, the atomic fraction of Si–N decreased with increasing x from 0 to 6.6 vol.%. For $x \geq 6.6$, the atomic fractions of both metal Si and Si–N were independent of x. These results indicate the progress of metal Si nitriding for $0 \leq x < 6.6$. The rapid increase in the N/Si ratio in Fig. 1(b) is considered to originate from the nitriding of metal Si. The effect of Si–O seems to be small since the atomic fraction of Si–O is much smaller than that of Si–N in all films.

Fig. 3(a) shows the diffraction image of Co_{19}–$(Si–N)_{81}$ films deposited in Ar-10 vol.%N_2 gas. The diffraction patterns showed the presence of hcp Co, but there were no observable patterns corresponding to Si_3N_4. Fig. 3 shows the TEM images of the films deposited in Ar- (b) 0, (c) 10, and (d) 30 vol.%N_2 gas. Insets display the high-resolution TEM images of the films. These diffraction images and TEM images revealed that Co_{19}–$(Si–N)_{81}$ films had a nanogranular structure composed of crystalline Co nanogranules embedded in an amorphous Si–N matrix. Fig. 3(e) shows the distribution of granule diameter, d, measured from TEM images of the films deposited in Ar-x vol.%N_2 gas ($0 \leq x \leq 30$). According to Fig. 3(e), the average diameter, d_{Ave}, of Co granules increased with increasing x from 0 (d_{Ave} = 1.6 nm) to 10 vol.% (d_{Ave} = 2.5 nm). In contrast, d_{Ave} slightly decreased for $x > 10$. Moreover, the films deposited in Ar-20 and 30 vol.%N_2 gas had a wider distribution of d than the films deposited in Ar-0 to 10 vol.%N_2 gas. Remarkably, Co granules in the film deposited in Ar-30 vol.%N_2 gas were aligned in the out-of-plane direction, which is different from those in the films deposited in Ar-0 and 10 vol.%N_2 gas, where Co granules homogeneously dispersed. This nanostructural evolution, varying with x, is schematically illustrated in Fig. 3(f).

B. Electric, Magnetic, and Magnetodielectric Properties

Fig. 4 shows the x dependence of (a) ρ and (b) magnetization with H = 800 kA/m, $4\pi M_{800\ \text{kA/m}}$. ρ increased with

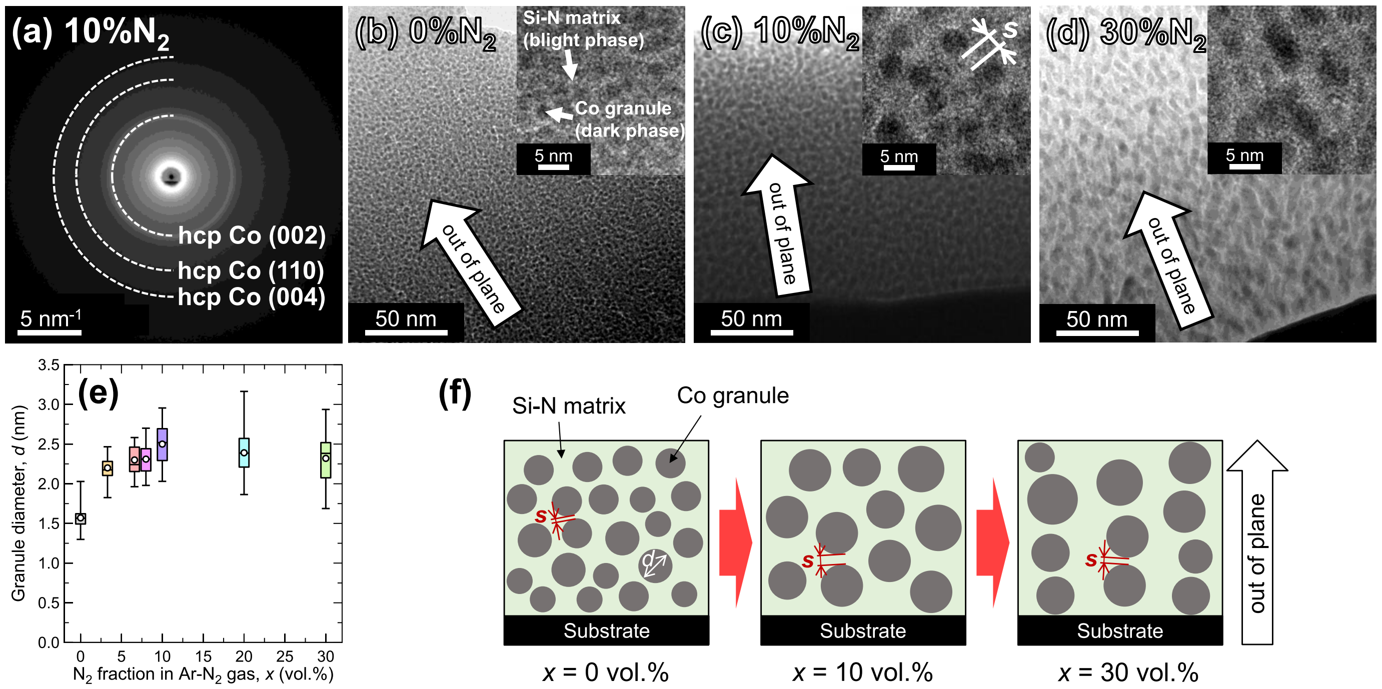

Fig. 3. (a) Diffraction patterns of Co_{19}–(Si–N)$_{81}$ films deposited in Ar-10 vol.%N_2 gas. TEM images of Co_{19}–(Si–N)$_{81}$ films deposited in Ar- (b) 0, (c) 10, and (d) 30 vol.%N_2 gas. (e) Distribution of granule diameter of the films deposited in Ar-x vol.%N_2 gas ($0 \leq x \leq 30$). (f) Schematic of morphological evolution in the films with different x value.

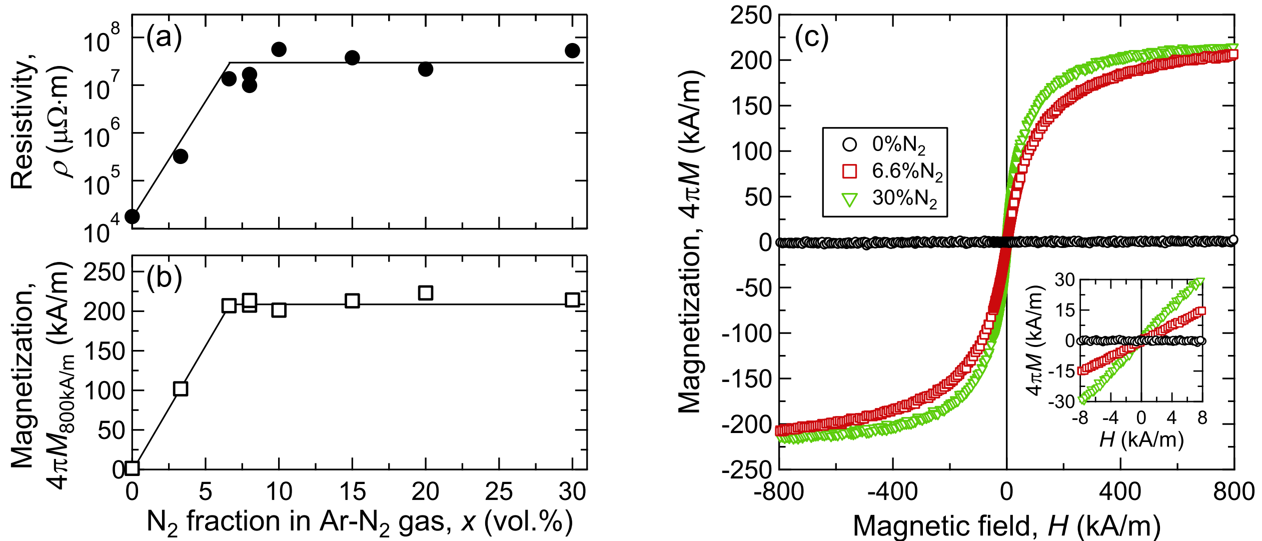

Fig. 4. N_2 gas fraction x dependence of (a) electrical resistivity ρ and (b) magnetization with $H = 800$ kA/m $4\pi M_{800\ \mathrm{kA/m}}$ of Co_{19}–(Si–N)$_{81}$ films. (c) Magnetization curves of the films deposited in Ar-0, 6.6, and 30 vol.%N_2 gas.

increasing x from 0 (10^4 $\mu\Omega\cdot$ m) to 6.6 vol.% (10^7 $\mu\Omega\cdot$ m) and became constant for $x \geq 6.6$. $4\pi M_{800\ \mathrm{kA/m}}$ also increased dramatically with increasing x from 0 ($4\pi M_{800\ \mathrm{kA/m}} = 1.4$ kA/m) to 6.6 vol.% ($4\pi M_{800\ \mathrm{kA/m}} = 208 \pm 15$ kA/m) and was saturated for $x \geq 6.6$. Herein, all Co_{19}–(Si–N)$_{81}$ nanogranular films exhibited superparamagnetism with almost zero coercivity, as shown in Fig. 4(c), which exhibits the magnetization curves of the films deposited in Ar-0, 6.6, and 30 vol.%N_2 gas. These rapid increases in ρ and $4\pi M_{800\ \mathrm{kA/m}}$ for $0 \leq x < 6.6$ are likely due to the nitriding of metal Si present in the films since metal Si in the Si–N matrix decreases the insulation of the matrix, and there are reports suggesting that the saturation magnetization of Co–Si alloys decreases as the Si content increases [23], [24].

Fig. 5(a) shows the frequency dependence of the real permittivity ε' with $H = 0$ (ε'_0) and 800 kA/m ($\varepsilon'_{800\ \mathrm{kA/m}}$). The ε' of the films before the relaxation frequency was much larger than that of amorphous Si_3N_4 thin films (6.5 [21]), since electrons oscillate between Co granule pairs by tunneling, and these granule pairs function like electric dipoles [12]. Thus, the relaxation frequency of ε' corresponds to the relaxation of the electron tunneling oscillation. The application of H leads

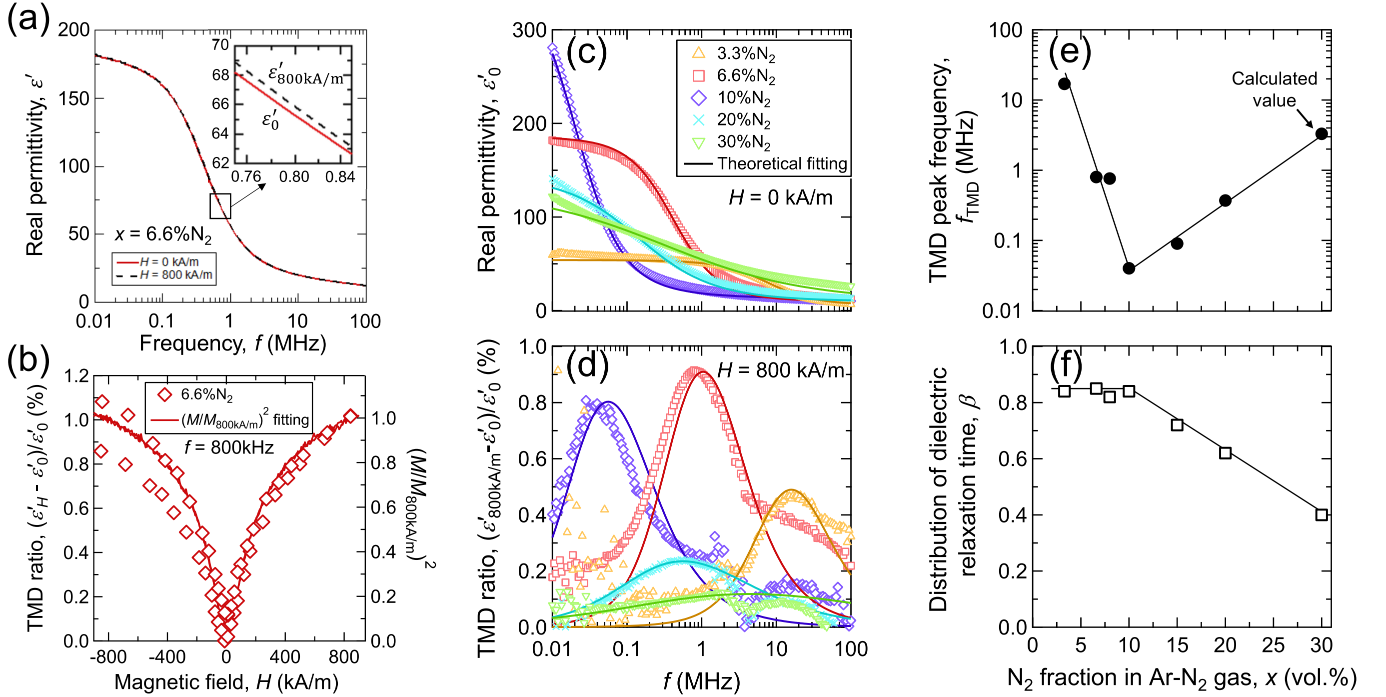

Fig. 5. (a) Frequency dependence of real permittivity ε' with $H = 0$ (ε'_0) and 800 kA/m ($\varepsilon'_{800\ \mathrm{kA/m}}$) and (b) magnetic field dependence of TMD effect in the film deposited in Ar-6.6 vol.%N_2 gas. Frequency dependence of (c) ε'_0 and (d) TMD response with $H = 800$ kA/m of the Co_{19}–$(Si–N)_{81}$ films deposited in Ar-3.3 to 30 vol.%N_2 gas. x dependence of (e) f_{TMD}, the TMD peak frequency, and (f) β, a measure of the distribution of the relaxation time of ε'_0.

to an increase in relaxation frequency, resulting in enhanced ε' near the relaxation frequency, as shown in the inserted figure in Fig. 5(a). Fig. 5(b) shows the H dependence of the TMD ratio in the film deposited in Ar-6.6 vol.%N_2 gas at a frequency of 800 kHz. ε' increases by applying H, and this behavior agrees well with $-(M/M_{800\ \mathrm{kA/m}})^2$ derived from the magnetization curve in Fig. 4(c). This result indicates that the enhancement of ε' is a consequence of the change in magnetization state of Co granules. Fig. 5(c) summarizes the frequency dependence of ε'_0 of the films deposited in Ar-3.3, 6.6, 10, 20, and 30 vol.%N_2 gas. The relaxation frequency decreased as x increased from 3.3 to 10 vol.%. On the other hand, it increased with increasing x from 10 to 30 vol.%. Fig. 5(d) shows the TMD response of the films against the frequency. The film deposited in pure Ar gas did not exhibit a TMD effect because of its low ρ and $4\pi M_{800\ \mathrm{kA/m}}$. TMD effect appeared for $x \geq 3.3$, and maximum TMD response was obtained in the film deposited in Ar-6.6 vol.%N_2 gas. Fig. 5(e) shows the x dependence of f_{TMD}, the frequency at which the peak of the TMD effect appears. According to Fig. 5(d) and (e), f_{TMD} decreased from 17 MHz to 40 kHz with increasing x for $3.3 \leq x \leq 10$. In contrast, for $10 < x \leq 30$, f_{TMD} increased from 40 kHz to 3.3 MHz (calc.) and became broader with increasing x. Solid lines in Fig. 5(c) and (d) are the theoretical fitting described as follows [12]:

$$\varepsilon'_H(\omega) = \varepsilon_\infty + \frac{1}{2}\Delta\varepsilon\left[1 - \frac{\sinh[\beta \ln(\omega\tau_r)]}{\cosh[\beta \ln(\omega\tau_r)] + \cos(\pi\beta/2)}\right] \tag{2}$$

where ε_∞ is the high-frequency dielectric constant; $\Delta\varepsilon$ is the dielectric strength; τ_r is the dielectric relaxation time, which is proportional to $1/(1 + P_T^2(M/M_s)^2)$, where P_T is spin polarization and M_s is saturation magnetization; and β is an exponent ($0 < \beta \leq 1$) representing a measure of the distribution of τ_r [25]. β also represents the distribution of intergranular spacing s [see the inset in Fig. 3(c)] since τ_r is determined by s. Fig. 5(f) shows the x dependence of β. β decreased with increasing x for $x > 10$, whereas it was almost constant for $x \leq 10$. This fitting result indicates that the distribution of s became broader with increasing x for $x \leq 10$.

We would like to discuss the origins of the shift in f_{TMD}. Our previous reports revealed f_{TMD} shifts to higher frequencies as s decreases and f_{TMD} shifts to lower frequencies as s increases [14], [15]. In Fig. 5(e), f_{TMD} shifted to lower frequencies with increasing x for $3.3 \leq x \leq 10$. This is attributed to the increase in s due to the increase in d under a constant Co composition [26], [27], as shown in Fig. 3(e) and (f). On the other hand, for $10 < x \leq 30$, f_{TMD} shifted to higher frequencies with increasing x, possibly owing to two reasons. One is the decrease in s in the out-of-plane direction (i.e., the direction of TMD measurement). As shown in Fig. 3(d) and (f), Co granules in the film deposited in Ar-30 vol.%N_2 gas were closely aligned in the out-of-plane direction, and s in that direction decreased. Another reason is the decrease in β for $10 < x \leq 30$, as shown in Fig. 5(f). In a previous study, we reported that f_{TMD} shifted to higher frequencies as β decreased [14]. For these two reasons, f_{TMD} would be high frequency for $x > 10$.

The experimental results combined with theoretical considerations reveal the previously overlooked importance of the sputtering atmosphere in the fine regulation of structural

evolution and the TMD effect, paving a new path to control the frequency characteristics of the TMD effect.

IV. Conclusion

We fabricated Co_{19}–(Si–N)$_{81}$ nanogranular films to realize the first TMD effect in nitride-based nanogranular films and to investigate the effect of N_2 gas fraction x in Ar–N_2 sputtering gas on the structure and TMD effect. Accordingly, we conclude the following.

1) All Co_{19}–(Si–N)$_{81}$ films had a nanogranular structure composed of crystallized Co nanogranules embedded in an amorphous Si–N matrix.
2) ρ and $4\pi M_{800\ \mathrm{kA/m}}$ increased with increasing x from 0 to 6.6 vol.%N_2, probably owing to the nitriding of metal Si in the films. For $x \geq 6.6$, ρ and $4\pi M_{800\ \mathrm{kA/m}}$ were independent of x since the nitriding of metal Si did not occur.
3) Co_{19}–(Si–N)$_{81}$ films showed a TMD effect for $x \geq 3.3$ owing to the improvements in ρ and $4\pi M_{800\ \mathrm{kA/m}}$. The maximum TMD effect (1.0%) was obtained in the film deposited in Ar-6.6 vol.%N_2 gas.
4) In the range of $3.3 \leq x \leq 10$, f_{TMD} shifted to lower frequencies as x increased, which can be attributed to the increase in granule diameter d, resulting in larger intergranular spacing s. Conversely, for the range of $10 < x \leq 30$, f_{TMD} shifted to higher frequencies, and the TMD peak became broader as x increased. These are due to the decrease in s in the out-of-plane direction and the decrease in β.

Acknowledgment

This work was supported in part by the Japan Society for the Promotion of Science (JSPS) KAKENHI under Grant 21K18810 and Grant 20H02447; and in part by the GIMRT Program of the Institute for Materials Research, Tohoku University, under Proposal 202112CRKEQ-0206. The authors would like to thank Ms. K. Omura and Dr. T. Miyazaki for their assistance with XPS experiments and TEM observation.

References

[1] H. Karamon, T. Masumoto, and Y. Makino, "Magnetic and electrical properties of Fe–B–N amorphous films (invited)," *J. Appl. Phys.*, vol. 57, no. 8, pp. 3527–3532, Apr. 1985.
[2] S. Ge et al., "Microstructure and magnetism of FeCo–SiO_2 nano-granular films for high frequency application," *J. Phys. D, Appl. Phys.*, vol. 40, no. 12, pp. 3660–3664, Jun. 2007.
[3] T. Li, X. Liu, J. Li, L. Pan, A. He, and Y. Dong, "Microstructure and magnetic properties of FeCoHfN thin films deposited by DC reactive sputtering," *J. Magn. Magn. Mater.*, vol. 547, Apr. 2022, Art. no. 168777.
[4] A. B. Pakhomov, X. Yan, and B. Zhao, "Giant Hall effect in percolating ferromagnetic granular metal-insulator films," *Appl. Phys. Lett.*, vol. 67, no. 23, pp. 3497–3499, Dec. 1995.
[5] J. C. Denardin, M. Knobel, X. X. Zhang, and A. B. Pakhomov, "Giant Hall effect in superparamagnetic granular films," *J. Magn. Magn. Mater.*, vol. 262, no. 1, pp. 15–22, May 2003.
[6] V. V. Rylkov et al., "Tunneling anomalous Hall effect in nanogranular CoFe-B-Al-O films near the metal-insulator transition," *Phys. Rev. B, Condens. Matter*, vol. 95, no. 14, Apr. 2017, Art. no. 144202.
[7] J. I. Gittleman, Y. Goldstein, and S. Bozowski, "Magnetic properties of granular nickel films," *Phys. Rev. B, Condens. Matter*, vol. 5, no. 9, pp. 3609–3621, May 1972.
[8] H. Fujimori, S. Mitani, and S. Ohnuma, "Tunnel-type GMR in metal-nonmetal granular alloy thin films," *Mater. Sci. Eng., B*, vol. 31, nos. 1–2, pp. 219–223, Apr. 1995.
[9] F. Xie et al., "Effect of nonuniform microstructure on magnetoresistance and field sensitivity in Co–MgO nanocomposite films," *Vacuum*, vol. 200, Jun. 2022, Art. no. 110976.
[10] N. Kobayashi, H. Masumoto, S. Takahashi, and S. Maekawa, "Optically transparent ferromagnetic nanogranular films with tunable transmittance," *Sci. Rep.*, vol. 6, no. 1, p. 34227, Sep. 2016.
[11] N. Kobayashi, K. Ikeda, B. Gu, S. Takahashi, H. Masumoto, and S. Maekawa, "Giant Faraday rotation in metal-fluoride nanogranular films," *Sci. Rep.*, vol. 8, no. 1, p. 4978, Mar. 2018.
[12] N. Kobayashi, H. Masumoto, S. Takahashi, and S. Maekawa, "Giant dielectric and magnetoelectric responses in insulating nanogranular films at room temperature," *Nature Commun.*, vol. 5, no. 1, p. 4417, Jul. 2014.
[13] Y. Cao, N. Kobayashi, Y.-W. Zhang, S. Ohnuma, and H. Masumoto, "Enhanced spin-dependent charge transport of Co-(Al-fluoride) granular nanocomposite by co-separate sputtering," *J. Appl. Phys.*, vol. 122, no. 13, Oct. 2017, Art. no. 133903.
[14] Y. Cao, A. Umetsu, N. Kobayashi, S. Ohnuma, and H. Masumoto, "Tunable frequency response of tunnel-type magneto-dielectric effect in Co–MgF_2 granular films with different content of Co," *Appl. Phys. Lett.*, vol. 111, no. 12, Sep. 2017, Art. no. 122901.
[15] Y. Cao, N. Kobayashi, S. Ohnuma, and H. Masumoto, "Tailored tunneling magneto-dielectric effects in Co–MgF_2 granular nanostructures by in-situ insertion of thin MgF_2 layers," *Appl. Phys. Lett.*, vol. 113, no. 2, Jul. 2018, Art. no. 022906.
[16] C. Wang, Y. Cao, N. Kobayashi, S. Ohnuma, and H. Masumoto, "Structure and tunneling magneto-dielectric properties of Co–SrF_2 nano-granular thin films," *AIP Adv.*, vol. 11, no. 8, Aug. 2021, Art. no. 085224.
[17] M. Kimura, Y. Cao, H. Kijima-Aoki, N. Kobayashi, S. Ohnuma, and H. Masumoto, "Tunneling magnetodielectric effect in Co–Al_2O_3 granular films," *Mater. Trans.*, vol. 63, no. 12, pp. 1677–1681, Oct. 2022.
[18] H. Kijima-Aoki, Y. Cao, N. Kobayashi, S. Takahashi, S. Ohnuma, and H. Masumoto, "Large magnetodielectric effect based on spin-dependent charge transfer in metal-insulator type Co-(BaF_2) nanogranular films," *J. Appl. Phys.*, vol. 128, no. 13, Oct. 2020, Art. no. 133904.
[19] Y. Cao, N. Kobayashi, S. Ohnuma, and H. Masumoto, "Tunnel-type magneto-dielectric effect and its annealing study in Co–SiO_2 granular films," *Mater. Trans.*, vol. 59, no. 4, pp. 585–589, 2018.
[20] C. J. Smithells, "Thermochemical data," in *Metals Reference Book*, vol. 1, 4th ed. London, Great Britain: Butterworth, 1967, pp. 240–244.
[21] S. M. Hu, "Properties of amorphous silicon nitride films," *J. Electrochem. Soc.*, vol. 113, no. 7, pp. 693–698, Jul. 1966.
[22] H. Bartzsch et al., "Electrical insulation properties of sputter-deposited SiO_2, Si_3N_4 and Al_2O_3 films at room temperature and 400 °C," *Phys. Status Solidi (A)*, vol. 206, no. 3, pp. 514–519, Mar. 2009.
[23] M. Velez et al., "Amorphous to polycrystalline transition in Co_xSi_{1-x} alloy thin films," *Eur. Phys. J. B*, vol. 41, pp. 517–524, Nov. 2004.
[24] Y. Cao, N. Kobayashi, S. Ohnuma, and H. Masumoto, "Large tunneling magneto-dielectric enhancement in Co(Fe)–MgF_2 granular films by minor addition of Si," *Appl. Phys. Lett.*, vol. 117, no. 7, Aug. 2020, Art. no. 072904.
[25] K. S. Cole and R. H. Cole, "Dispersion and absorption in dielectrics I. Alternating current characteristics," *J. Chem. Phys.*, vol. 9, no. 4, pp. 341–351, Apr. 1941.
[26] P. Sheng, B. Abeles, and Y. Arie, "Hopping conductivity in granular metals," *Phys. Rev. Lett.*, vol. 31, no. 1, pp. 44–47, Jul. 1973.
[27] J. S. Helman and B. Abeles, "Tunneling of spin-polarized electrons and magnetoresistance in granular Ni films," *Phys. Rev. Lett.*, vol. 37, no. 21, pp. 1429–1432, Nov. 1976.